

# Optically Active 4- and 5-Coordinate Transition Metal Complexes of Bifurcated Dipeptide Schiff Bases

Robin Polt,\* Brian D. Kelly, Brian D. Dangel, Udaya Bhaskar Tadikonda, Regina E. Ross, Arnold M. Raitsimring, and Andrei V. Astashkin

Department of Chemistry, The University of Arizona, Tucson, Arizona 85721

Received September 3, 2002

Symmetrical and unsymmetrical benzophenone Schiff bases of bifurcated dipeptides [e.g.,  $\text{Ar}_2\text{C}=\text{N}-\text{CHR}^1-\text{CONH}-\text{HNCO}-\text{CHR}^2-\text{N}=\text{CAr}_2$ ] have been synthesized using Boc methodology. These ligands may be regarded as chiral porphyrin mimics because of the  $\alpha$ -carbons of the amino acids. The Schiff bases function as effective ligands for transition metals, particularly the late transition metals Ni(II), Cu(II), and Zn. Upon metal insertion, there is loss of the amide protons, resulting in  $\text{N}_4$  chelating ligands that retain the amino acid based chirality as well as newly generated metal-centered chirality, which for the Ni(II) complexes have been shown by X-ray analysis to be  $\Delta$  (left-handed helix) if the amino acids are S. For Ni(II) and Cu(II), metal insertion results in highly colored complexes and is easily followed by UV-vis spectrophotometry. Several Ni(II) complexes were also characterized by  $^1\text{H}$  NMR. Co(II) and Mn(II) complexes were characterized by CW EPR. Two Cu(II) complexes, **7f**·Cu<sup>II</sup> and **7k**·Cu<sup>II</sup>, were characterized by EPR (ENDOR and ESEEM), which clearly showed the pentacoordinate nature of **7k**·Cu<sup>II</sup>.

## Introduction

Metalloenzymes are capable of many remarkable regio- and stereoselective transformations in vivo, to which synthetic organic chemistry can presently only aspire.<sup>1</sup> These aspirational goals are extremely beneficial, serving originally to stimulate synthetic studies to produce enzyme “mimics” that help unravel the principles of metalloenzyme function,<sup>2</sup> and have been applied directly to problems in enantioselective catalysis more recently.<sup>3</sup> Complexes of Ni(II), Cu(II), Co(II), and Pd(II) and picolinamide based ligands (e.g., **1**, Figure 1) were characterized some time ago,<sup>4</sup> and there is growing interest in nonplanar salen complexes.<sup>5</sup> As a con-

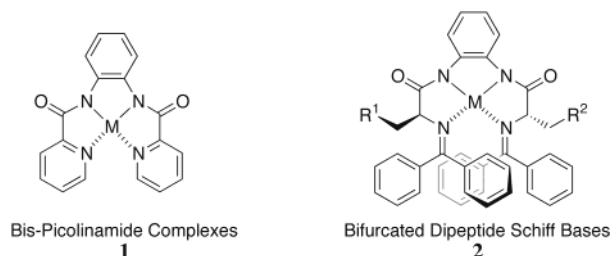


**Figure 1.** Metal-centered chirality. Achiral Nomoyama complexes **1**. The metal-centered chirality of **2** is enhanced by the steric interactions of the overlapping aryl groups.

sequence of the modular character, peptides are of particular interest as ligands for catalyst libraries.<sup>6</sup> Recently, we have begun to explore the catalytic activity of enantiomerically pure transition metal complexes **2**,<sup>7</sup> which could be regarded as porphyrin mimics,<sup>8</sup> or alternatively as bifurcated peptide complexes.<sup>9</sup>

## Experimental Section

**General Procedure for Preparation of  $\text{C}_2$ -Symmetric Bifurcated Dipeptides (4a, 4c, 4e–g).** Phenylenediamine (1 equiv) was

\* To whom correspondence should be addressed. E-mail: polt@u.arizona.edu.

- (1) (a) Ermler, U.; Grabarse, W.; Shima, S.; Goubeaud, M.; Thauer, R. K. *Curr. Opin. Struct. Biol.* **1998**, *8*, 749–758. (b) Gray, H. B.; Malmstrom, B. G.; Williams, R. J. P. *JBIC, J. Biol. Inorg. Chem.* **2000**, *5*, 551–559.
- (2) (a) Pinto, A. L.; Hellinga, H. W.; Caradonna, J. P. *Proc. Natl. Acad. Sci. U.S.A.* **1997**, *94*, 5562–5567. (b) Watt, R. K.; Ludden, P. W. *Cell. Mol. Life Sci.* **1999**, *56*, 604–625. (c) Hage, R.; Kerschner, J. *Trends Inorg. Chem.* **1998**, *5*, 145–159. (d) Lippard, S. J.; Berg, J. M. *Curr. Opin. Chem. Biol.* **2000**, *4*, 137–139. (e) Henderson, R. A. *J. Chem. Soc., Dalton Trans.* **1995**, 503–11.
- (3) (a) Pierre, J.-L. *Chem. Soc. Rev.* **2000**, *29*, 251–257. (b) Fenton, D. E. *Chem. Soc. Rev.* **1999**, *28*, 159–168. (c) Berkessel, A. *Sel. React. Met.-Act. Mol., Proc. Symp.*, 3rd **1998**, 25–33. (d) Costas, M.; Chen, K.; Que, L. *Coord. Chem. Rev.* **2000**, *200*–202, 517–544. (e) Robert, A.; Meunier, B. *Biomimetic Oxid. Catal. Transition Met. Complexes* **2000**, 543–562.
- (4) Nonoyama, M.; Yamasaki, K. *Inorg. Chim. Acta* **1973**, *7*, 373–7.

- (5) Yamada, S. *Coord. Chem. Rev.* **1999**, *190*–192, 537–555.
- (6) Severin, K.; Bergs, R.; Beck, W. *Angew. Chem., Int. Ed.* **1998**, *37*, 1635–1654.
- (7) (a) Dangel, B.; Clarke, M.; Haley, J.; Sames, D.; Polt, R. *J. Am. Chem. Soc.* **1997**, *119*, 10865–6. (b) Dangel, B. D.; Polt, R. *Org. Lett.* **2000**, *2*, 3003–6.

dissolved in DMF (dimethylformamide) (200 mL). DIEA (3 equiv) was added in a single portion and the reaction mixture cooled to 0 °C. Boc-amino acid (2.2 equiv) and BOP (2.5 equiv) were added in one portion. The solution was allowed to warm to room temperature for 24 h, after which complete conversion of starting material was observed by TLC. The reaction was diluted with EtOAc and washed with 1% NaCl (3 × 200 mL), 1 M HCl (2 × 200 mL), 1% NaCl (1 × 200 mL), saturated NaHCO<sub>3</sub> (2 × 200 mL), and saturated NaCl (1 × 200 mL). The organic layer was dried over MgSO<sub>4</sub>, filtered, and reduced to a foam in vacuo.

**General Procedure for One-Pot Preparation of Non-C<sub>2</sub>-Symmetric Bifurcated Dipeptides (4b, 4d, 4h–k).** Phenylenediamine (1 equiv) was dissolved in DMF (200 mL). DIEA (1.5 equiv) was added in a single portion and the reaction mixture cooled to 0 °C. The first boc-amino acid (0.97 equiv) and BOP (1.25 equiv) were added in one portion. The reaction was held at 0 °C for 45 min, by which time TLC showed complete mono-acylation. The second boc-amino acid (1.1 equiv) was added in one portion followed by addition of BOP (1.25 equiv) and DIEA (1.5 equiv). The solution was allowed to warm to room temperature for 24 h, after which complete conversion of starting material was observed by TLC. The reaction was diluted with EtOAc and washed with 1% NaCl (3 × 200 mL), 1 M HCl (2 × 200 mL), 1% NaCl (1 × 200 mL), saturated NaHCO<sub>3</sub> (2 × 200 mL), and saturated NaCl (1 × 200 mL). The organic layer was dried over MgSO<sub>4</sub>, filtered, and reduced to a foam in vacuo.

**General Procedure for Boc Deprotection (5a–m).** Compound 4(a–m) was dissolved in 50 mL of anhydrous MeOH and chilled to 0 °C. In a separate flask, 50 mL of MeOH was chilled to 0 °C. AcCl (4 equiv) was added slowly. The resultant methanolic HCl solution was added to the chilled reaction mixture dropwise over 30 min. The reaction mixture was allowed to warm to room temperature for 24 h. After all the starting material had been consumed, as judged by TLC, MeOH was removed by rotary evaporation. The residual HCl was removed by dissolving the residue in MeOH and subsequent rotary evaporation (5 × 200 mL). This material was placed in vacuo until a brittle foam was obtained, and then triturated in Et<sub>2</sub>O until a fine suspension was achieved. The HCl salt was collected by filtration and was dried overnight under vacuum and over P<sub>2</sub>O<sub>5</sub>.

**General Procedure for Schiff Base Formation (6a–m).** Compound 5(a–m) was suspended in 60 mL of CH<sub>2</sub>Cl<sub>2</sub>. Benzophenone imine (2.05 equiv) was added in a single portion. The resultant slurry was stirred at room temperature for 12 h. Upon completion, the reaction was diluted with 100 mL of CH<sub>2</sub>Cl<sub>2</sub> and washed with saturated NaHCO<sub>3</sub> (3 × 100 mL). The organic layer was taken, dried over K<sub>2</sub>CO<sub>3</sub>, filtered, and concentrated in vacuo.

**2(S)-(Benzhydrylidene-amino)-N-{2-[2(S)-(benzhydrylidene-amino)-3-phenyl-propionylamino]-phenyl}-3-phenyl-propionamide-nickel(II) Complex (7f·Ni<sup>II</sup>).** In a 100 mL glass round-bottom flask equipped with a reflux condenser, 6f (300 mg, 0.411 mmol) was dissolved in methanol (10 mL) and triethylamine (508 mg,

0.7 mL, 5.02 mmol). NiBr<sub>2</sub> (900 mg, 4.12 mmol) was added, and the slurry was heated to reflux for 30 h. A green precipitate formed upon heating (believed to be nickel oxide). The progress of the reaction was monitored by TLC (70% toluene/30% ethyl acetate). The green solid was filtered and discarded. The mother liquor was stripped to a solid by rotary evaporation. The brown residue was dissolved in methylene chloride (40 mL) and extracted with a 10% NaHCO<sub>3</sub> solution (2 × 40 mL). The organic layer was dried over anhydrous CaCl<sub>2</sub>, filtered, and stripped to a solid. Purification by flash chromatography (70% toluene/30% ethyl acetate) and subsequent vapor crystallization (ethyl acetate/hexane) gave 209 mg of 7f·Ni<sup>II</sup> as maroon crystals in an overall 65% yield. Mp > 200 °C. [α]<sub>D</sub> = (−)486 (2.87 × 10<sup>−3</sup> g/100 mL in MeOH). IR (KBr pellet): 3056, 1642, 1570, 1483, 1448, 1373, 1029, 749, 705 cm<sup>−1</sup>. <sup>1</sup>H NMR (CDCl<sub>3</sub>) δ (ppm): 6.3–8.5 (m, 34 H), 3.8–4.0 (m, 4 H), 2.4–2.5 (dd, J<sub>AX</sub> = 12 Hz, J<sub>BX</sub> = 3.2 Hz, 2 H). <sup>13</sup>C NMR (CDCl<sub>3</sub>) δ (ppm): 182, 174, 119–142, 78, 44. UV–vis λ<sub>max</sub> [DCM (dichloromethane)]: 234 nm (ε = 33670 M<sup>−1</sup> cm<sup>−1</sup>, A = 2.002), 254 nm (ε = 31954 M<sup>−1</sup> cm<sup>−1</sup>, A = 1.90), 370 nm (ε = 4901 M<sup>−1</sup> cm<sup>−1</sup>, A = 0.29141). FAB MS = 787.2603 g/mol.

**2(S)-(Benzhydrylidene-amino)-N-{2-[2(S)-(benzhydrylidene-amino)-3-phenyl-propionylamino]-phenyl}-3-phenyl-propionamide-copper(II) Complex (7f·Cu<sup>II</sup>).** In a 100 mL glass round-bottom flask, 6f (100 mg, 0.137 mmol) was dissolved in DMF (5 mL) and DBU (1,8-diazabicyclo[5.4.0]undec-7-ene) (72.3 mg, 0.457 mmol). CuCl<sub>2</sub> was added to the solution. The resulting brown solution was stirred at room temperature for 10 min. The progress of the reaction was monitored by TLC (70% toluene/30% ethyl acetate). The DMF was azeotropically removed with toluene. The resulting residue was dissolved in DCM (10 mL) and extracted with 10% NaHCO<sub>3</sub> (2 × 30 mL). A second extraction with saturated NaHCO<sub>3</sub> (125 mL), followed by a brine wash, was performed. The organic layer was dried over K<sub>2</sub>CO<sub>3</sub>, filtered, and stripped to a solid. Purification by flash chromatography and subsequent vapor crystallization from ethyl acetate and hexanes gave 72.1 mg of 6f as brown crystals in an overall 60% yield. Mp > 200 °C. [α]<sub>D</sub> = (−)1920 (1.87 × 10<sup>−3</sup> g/100 mL in CHCl<sub>3</sub>). IR (KBr pellet): 3056, 2925, 1623, 1570, 1474, 1460, 1380, 1291, 758, 700 cm<sup>−1</sup>. UV–vis λ<sub>max</sub> (DCM): 222 nm (ε = 41 834 M<sup>−1</sup> cm<sup>−1</sup>, A = 1.0153), 244 nm (ε = 47 005 M<sup>−1</sup> cm<sup>−1</sup>, A = 1.1408), 272 nm (ε = 32 528 M<sup>−1</sup> cm<sup>−1</sup>, A = 0.78946), 340 nm (ε = 3496 M<sup>−1</sup> cm<sup>−1</sup>, A = 0.08485). FAB MS = 791.2463 g/mol.

**2(S)-(Benzhydrylidene-amino)-N-{2-[2(S)-(benzhydrylidene-amino)-3-phenyl-propionylamino]-phenyl}-3-phenyl-propionamide-zinc(II) Complex (7f·Zn<sup>II</sup>).** In a flame-dried 50 mL glass round-bottom flask, 6f (219 mg, 0.3 mmol) was dissolved in 3 mL of freshly distilled THF. To the clear homogeneous solution, a 0.5 M Et<sub>2</sub>Zn solution in THF (0.64 mL, 0.32 mmol) was added in a single portion. The resultant reaction mixture was heated to reflux for 1 h. The Zn complex is relatively stable, and its formation can be monitored by TLC (80% hexanes/20% ethyl acetate). Two UV active spots are observed corresponding to the complex (R<sub>f</sub> = 0.2) and 6f (R<sub>f</sub> = 0.75) which is generated from the hydrolysis of the complex during the TLC development.

**Determination of Kinetics of Nickel(II) Insertion.** A 100 mL three neck round-bottom flask was equipped with a reflux condenser, glass stopper, and septum. NiBr<sub>2</sub> (1.25 × 10<sup>−5</sup> mol) and 6f (1.25 × 10<sup>−5</sup> mol) were dissolved in 60 mL of MeOH and heated to reflux under an argon atmosphere. The initial UV–vis spectrum was measured, followed by addition of NEt<sub>3</sub> (3.12 × 10<sup>−6</sup> mol) at time zero. The UV–vis spectra were measured using a fiber optic dip probe attached to a SI440 spectrophotometer (Spectral Instruments, Inc., Tucson, Arizona). Full spectra (200–900 nm) were

- (8) (a) Nanthakumar, A.; Miura, J.; Diltz, S.; Lee, C.-K.; Aguirre, G.; Ortega, R.; Ziller, J. W.; Walsh, P. J. *Inorg. Chem.* **1999**, *38*, 3010–13. (b) Hsiao, Y.; Hegedus, L. S. *J. Org. Chem.* **1997**, *62*, 3586–91. (c) Schaus, W. E.; Larrow, J. F.; Jacobsen, E. N. *J. Org. Chem.* **1997**, *62*, 4197–4199. (d) Kobayashi, N.; Kabayashi, Y.; Osa, T. *J. Am. Chem. Soc.* **1993**, *115*, 10994–5. (e) Busch, D. H. *Acc. Chem. Res.* **1978**, *11*, 392–400.
- (9) (a) Bair, M. L.; Larsen, E. M. *J. Am. Chem. Soc.* **1971**, *93*, 1140–1148. (b) Gergely, A.; Farkas, E. *J. Chem. Soc., Dalton Trans.* **1977**, 381–386. (c) Raghunath, P.; Agarwal; Perrin, D. D. *J. Chem. Soc., Dalton Trans.* **1977**, 53–57.

**Table 1.** Summary of Crystallographic Details for **7b·Ni<sup>II</sup>**, ***p*-MeO-7b·Ni<sup>II</sup>**, **7f·Ni<sup>II</sup>**, ***p*-MeO-7f·Ni<sup>II</sup>**, ***rac*-7g·Ni<sup>II</sup>**, **CH<sub>2</sub>Cl<sub>2</sub>-7g·Ni<sup>II</sup>**, **7l·Ni<sup>II</sup>**, **11**

	<b>7b·Ni<sup>II</sup></b>	<b><i>p</i>-MeO-7b·Ni<sup>II</sup></b>	<b>7f·Ni<sup>II</sup></b>	<b><i>p</i>-MeO-7f·Ni<sup>II</sup></b>	<b><i>rac</i>-7g·Ni<sup>II</sup></b>	<b>CH<sub>2</sub>Cl<sub>2</sub>-7g·Ni<sup>II</sup></b>	<b>7l·Ni<sup>II</sup></b>	<b>11</b>
unique reflns (total)	8500 (23421)	7878 (42284)	15136 (15136)	10513 (39718)	7526 (37222)	10774 (12178)	17022 (22997)	7515 (28537)
$\theta_{\max}$ (deg)	29.32	25.77	24.97	28.63	28.26	27.23	28.338	24.455
empirical formula	C <sub>43</sub> H <sub>34</sub> N <sub>4</sub> NiO <sub>2</sub>	C <sub>47</sub> H <sub>42</sub> N <sub>4</sub> NiO <sub>6</sub>	C <sub>50</sub> H <sub>40</sub> N <sub>4</sub> NiO <sub>2</sub>	C <sub>54</sub> H <sub>48</sub> N <sub>4</sub> NiO <sub>6</sub>	C <sub>38</sub> H <sub>32</sub> N <sub>4</sub> NiO <sub>4</sub>	C <sub>38</sub> H <sub>32</sub> N <sub>4</sub> NiO <sub>4</sub>	C <sub>42</sub> H <sub>36</sub> N <sub>4</sub> NiO <sub>6</sub>	C <sub>41</sub> H <sub>33</sub> N <sub>3</sub> O
$M_r$	697.45	902.48	787.572	907.67	709.85	667.39	751.47	583.70
cryst syst	orthorhombic	monoclinic	orthorhombic	orthorhombic	monoclinic	triclinic	triclinic	orthorhombic
space group	<i>P</i> 2 <sub>1</sub> 2 <sub>1</sub> 2 <sub>1</sub>	<i>P</i> 2 <sub>1</sub> /c	<i>P</i> 2 <sub>1</sub> 2 <sub>1</sub> 2 <sub>1</sub>	<i>P</i> 2 <sub>1</sub> 2 <sub>1</sub> 2 <sub>1</sub>	<i>P</i> 2 <sub>1</sub> /c	<i>P</i> 1	<i>P</i> 1	<i>P</i> 2 <sub>1</sub> 2 <sub>1</sub> 2 <sub>1</sub>
<i>a</i> (Å)	9.3318(7)	13.4825(13)	17.259(4)	12.4041(8)	21.888(2)	8.6240(10)	8.629(2)	9.7799(6)
<i>b</i> (Å)	15.6129(12)	11.5511(11)	14.290(3)	13.5171(9)	14.0327(14)	10.1739(12)	9.665(3)	17.6968(10)
<i>c</i> (Å)	23.3240(18)	26.762(3)	34.939(7)	26.1586(17)	10.7457(11)	18.951(2)	23.136(6)	18.0760(10)
$\alpha$ (deg)	90	90	90	90	90	94.644(2)	79.747(9)	90
$\beta$ (deg)	90	99.012(2)	90	90	101.070	99.792(2)	88.743(9)	90
$\gamma$ (deg)	90	90	90	90	90	91.997(2)	89.707(7)	90
$V_c$ (Å <sup>3</sup> )	3398.2(4)	4116.4(7)	8617(3)	4385.9(5)	3239.1(6)	1631.2(3)	1898.3(9)	3128.5(3)
$D_c$ (Mg/m <sup>3</sup> )	1.363	1.456	1.282	1.375	1.456	1.359	1.463	1.239
<i>Z</i>	4	4	4	4	4	2	2	4
$\mu$ (Mo K $\alpha$ ) (mm <sup>-1</sup> )	0.616	0.659	0.499	0.501	0.731	0.642	0.708	0.075
$R1^a$ [ $I \geq 2\sigma(I)$ data]	0.0457	0.0914	0.068	0.0366	0.0562	0.0339	0.0486	0.0432
wR2	0.0654	0.2146	0.933	0.0711	0.1135	0.0658	0.0933	0.0728
GOF	0.808	0.943	0.994	0.920	0.926	0.955	0.953	0.881
larg diff peak, hole (e Å <sup>-3</sup> )	+0.741, -0.383	+0.607, -0.673	+0.336, -0.214	+0.289, -0.304	+0.653, -0.560	+0.513, -0.228	+0.708, -0.771	+0.193, -0.155

$$^a R1 = \sum ||F_o| - |F_c|| / \sum |F_o|; wR2 = \{\sum [w(F_o^2 - F_c^2)] / \sum [w(F_o^2)]\}^{1/2}.$$

measured at regular intervals (every 15 min for the first hour and every 30 min after that) by inserting the probe through the septum. The insertion of Ni<sup>II</sup> was monitored by observing the increase in absorbance of the band due to **7f·Ni<sup>II</sup>** at 370 nm.

**X-ray Structure Determination of **7b·Ni<sup>II</sup>**, ***p*-MeO-7b·Ni<sup>II</sup>**, **7f·Ni<sup>II</sup>**, ***p*-MeO-7f·Ni<sup>II</sup>**, ***rac*-7g·Ni<sup>II</sup>**, **CH<sub>2</sub>Cl<sub>2</sub>-7g·Ni<sup>II</sup>**, **7l·Ni<sup>II</sup>**, **11**.** Crystal, data collection, and refinement parameters are given in Table 1. Suitable crystals were mounted in a random orientation on a thin glass fiber. X-ray diffraction data were collected at 170-(2) K on a Bruker SMART 1000 CCD detector with Mo K $\alpha$  radiation ( $\lambda = 0.71073$  Å). The frames were integrated using the Bruker SAINT<sup>10</sup> package's narrow frame algorithm. Empirical absorption and decay corrections were applied using the program SADABS (Sheldrick 1997). The structure solutions were achieved utilizing direct methods followed by Fourier synthesis using SHELXS in the Bruker SHELXTL<sup>11</sup> software package. Refinements were performed using SHELXL and illustrations made using XP. A complete list of bond distances and angles is available for all compounds in CIF format as Supporting Information.

## Ligand Synthesis

The Schiff base ligands are easily accessible via the *t*-Boc-protected intermediates (Table 2, Scheme 1). The *t*-Boc amino acids (R<sup>1</sup>) can be reacted with *ortho*-phenylenediamine to provide the mono-acylated intermediates, **3**. Mono-acylation is favored because of large differences in the acylation rates for the diamine versus acylation rates for the mono-acylated product, which possesses an unfavorable hydrogen bonding pattern and proceeds slowly at 0 °C. Subsequent acylation with a second *t*-Boc amino acid (R<sup>2</sup>) proceeded at acceptable rates at RT (room temperature) to provide the

**Table 2.** Yields for Bifurcated *t*-Boc Protected Dipeptides

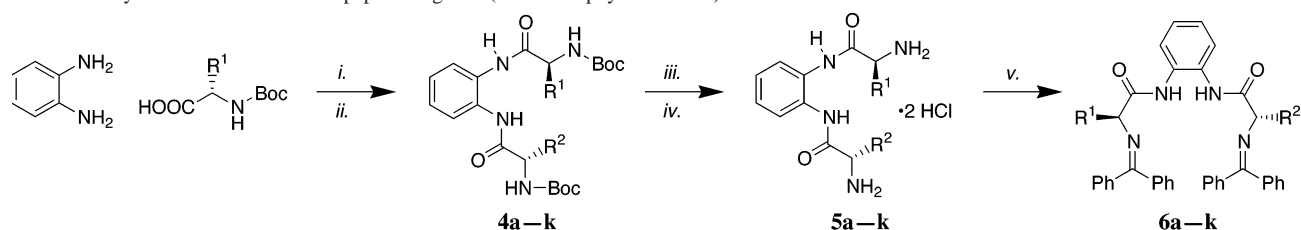
entry	amino acids	R <sup>1</sup> (PG <sup>1</sup> ), R <sup>2</sup> (PG <sup>2</sup> )	yield ( <b>4</b> )
<b>a</b>	Gly, Gly	H, H	92%
<b>b</b>	Gly, Phe	H, CH <sub>2</sub> Ph	99%
<b>c</b>	Ala, Ala	CH <sub>3</sub> , CH <sub>3</sub>	97%
<b>d</b>	Ala, Phe	CH <sub>3</sub> , CH <sub>2</sub> Ph	85%
<b>e</b>	Val, Val	CH(CH <sub>3</sub> ) <sub>2</sub> , CH(CH <sub>3</sub> ) <sub>2</sub>	90%
<b>f</b>	Phe, Phe	CH <sub>2</sub> Ph, CH <sub>2</sub> Ph	98%
<b>g</b>	Ser, Ser	CH <sub>2</sub> OBn, CH <sub>2</sub> OBn	98%
<b>h</b>	Phe, Ser	CH <sub>2</sub> Ph, CH <sub>2</sub> OBn	93%
<b>i</b>	Phe, Cys	CH <sub>2</sub> Ph, CH <sub>2</sub> STrt	88%
<b>j</b>	Phe, His	CH <sub>2</sub> Ph, CH <sub>2</sub> ImDNP	93%
<b>k</b>	Phe, <i>N</i> -Bn(His)	CH <sub>2</sub> Ph, CH <sub>2</sub> ImBn	73%

*t*-Boc-protected dipeptide **4**. This sequence can be performed with or without isolation of the mono-acylated intermediates **3**. The yields for these reactions were generally excellent, with the exception of S-trityl-protected *t*-Boc-cysteine (44% for R<sup>1</sup> = Phe, R<sup>2</sup> = S-trityl-Cys), probably because of the extreme bulk exhibited by this side chain. Yields were increased when the bulkier of the two residues was coupled first. Cleavage of the Boc groups from **4** was accomplished with methanolic HCl, which was generated in situ from AcCl and MeOH. The resulting salts **5**·2HCl were conveniently stored as white or off-white crystalline solids.

Condensation of the dipeptide salts **5**·2HCl with commercially available (redistilled) Ph<sub>2</sub>C=NH or the corresponding *para*-methoxy-substituted ketimine, (*p*-MeOPh)<sub>2</sub>C=NH, was accomplished under a variety of conditions. For aliphatic side chains, the solvents CH<sub>2</sub>Cl<sub>2</sub>, ClCH<sub>2</sub>CH<sub>2</sub>Cl, or CH<sub>3</sub>CN generally worked well without catalysis (Tables 2 and 3). For the bifurcated dipeptides bearing more polar side chain residues, cosolvent mixtures of CH<sub>3</sub>CN/DMF or the solvent NMP (*N*-methylpyrrolidinone) was used. Alternatively, free bases **5** could be condensed in the presence of a catalytic amount of a protic acid (e.g., camphorsulfonic acid, HBr), or in the presence of BF<sub>3</sub>·Et<sub>2</sub>O. In most cases, the

(10) SAINT, V5; Program for reduction of data collected on Bruker AXS CCD area detector systems; Bruker Analytical X-ray Systems: Madison, WI, 1997.

(11) SHELXTL, V5; Program suite for solution and refinement of crystal structures; Bruker Analytical X-ray Systems: Madison, WI, 1997.

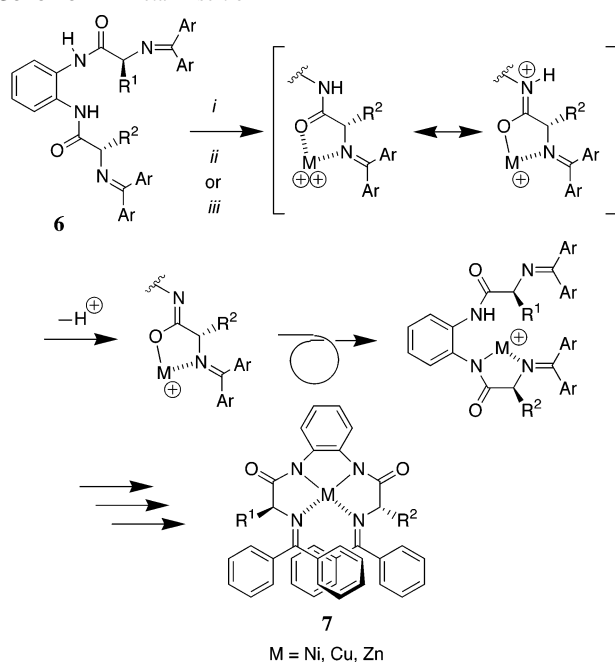
**Scheme 1.** Synthesis of Bifurcated Dipeptide Ligands (Chiral Porphyrin Mimics)<sup>a</sup>

<sup>a</sup> Reagents: i, BOP, <sup>i</sup>Pr<sub>2</sub>NEt, DMF, 0 °C, 30 min; ii, *t*-Boc-NH-CHR<sup>2</sup>COOH, BOP, <sup>i</sup>Pr<sub>2</sub>NEt, DMF, RT, 5–8 h; iii, AcCl, MeOH, 0 °C, inverse addition; iv, for side chain modifications, see Experimental Section; v, Ph<sub>2</sub>C=NH, CH<sub>2</sub>Cl<sub>2</sub>, RT.

**Table 3.** Yields for Schiff Base Ligands and Intermediates

entry	amino acids	R <sup>1</sup>	R <sup>2</sup>	yield (5)	yield <sup>a</sup> (6)	[α] <sub>D</sub> (6) c ≈ 1, CHCl <sub>3</sub>
a	Gly, Gly	H	H	99%	49%	
b	Gly, Phe	H	CH <sub>2</sub> Ph	92%	23%	(–)–104°
c	Ala, Ala	CH <sub>3</sub>	CH <sub>3</sub>	98%	45%	(+)-50°
d	Ala, Phe	CH <sub>3</sub>	CH <sub>2</sub> Ph	98%	73%	(–)–22° <sup>b</sup>
e	Val, Val	CH(CH <sub>3</sub> ) <sub>2</sub>	CH(CH <sub>3</sub> ) <sub>2</sub>	98%	69%	(–)–20°
f	Phe, Phe	CH <sub>2</sub> Ph	CH <sub>2</sub> Ph	99%	72%	(–)–159°
g	Ser, Ser	CH <sub>2</sub> OH	CH <sub>2</sub> OH	99%	98%	(+)-11°
h	Phe, Ser	CH <sub>2</sub> Ph	CH <sub>2</sub> OH	99%	92%	(–)–90°
i	Phe, Cys	CH <sub>2</sub> Ph	CH <sub>2</sub> SH	93%	58%	(–)–38°
j	Phe, His	CH <sub>2</sub> Ph	CH <sub>2</sub> Im	88%	79%	(–)–109°
k	Phe, <i>N</i> -Bn-His	CH <sub>2</sub> Ph	CH <sub>2</sub> ImBn	80%	79%	(–)–80°
l <sup>c</sup>	Ser, Ser	CH <sub>2</sub> OAc	CH <sub>2</sub> OAc		98%	(+)-41°

<sup>a</sup> Unoptimized yields for **6a–k**. <sup>b</sup> Measured in CH<sub>3</sub>CN. <sup>c</sup> Via acylation of **6g**.

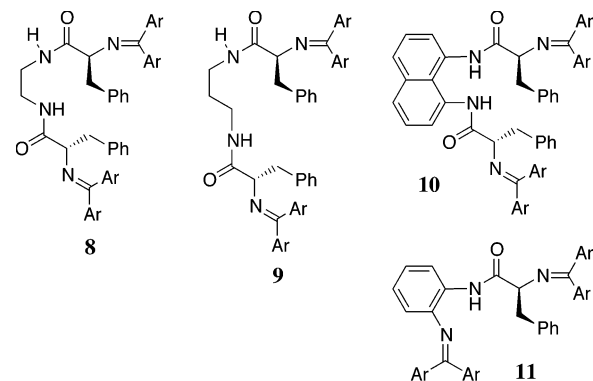
**Scheme 2.** Metal Insertion<sup>a</sup>

<sup>a</sup> Reagents: i, NiBr<sub>2</sub>, Et<sub>3</sub>N, THF, 12 h, reflux; ii, CuCl<sub>2</sub>, DBU, DMF, 1 min, RT; iii, Et<sub>2</sub>Zn, THF, 1 h, reflux.

resultant Schiff bases ligands **6** were isolated as glassy solids after column chromatography.

### Metal Insertion

Insertion of Cu(II) proceeded readily at RT with CuCl<sub>2</sub> in the presence of DBU in DMF or CH<sub>3</sub>CN to provide stable, highly colored, EPR-active complexes (Scheme 2). Insertion of Ni(II) as NiBr<sub>2</sub> required higher temperatures (refluxing

**Figure 2.** Other diamine analogues of **6f**.

THF) in the presence of NEt<sub>3</sub> to produce maroon crystals of a square planar complex. Zinc insertion was accomplished by heating the ligand in the presence of Et<sub>2</sub>Zn in either THF or toluene under argon.

Purification of the Cu(II) and Ni(II) complexes was easily accomplished with silica gel chromatography. The Zn complexes could be subjected to TLC with some streaking but were too polar for column chromatography. The metals Co(II) (CoCl<sub>2</sub>) and Mn(II) (Mn(OAc)<sub>2</sub>) formed complexes with **6k**, and were characterized by CW EPR, but did not crystallize. All of the metals produced visible M<sup>+</sup> ions of the insertion product using FAB MS. The insertion reaction was tolerant of a wide variety of amino acid side chains: R<sup>1</sup>, R<sup>2</sup> = –H, –CH<sub>3</sub>, –CH<sub>2</sub>Ph, –CH(CH<sub>3</sub>)<sub>2</sub>, –CH<sub>2</sub>OH, –CH<sub>2</sub>SH, –CH<sub>2</sub>OBn, –CH<sub>2</sub>SC(Ph)<sub>3</sub>, –CH<sub>2</sub>–imidazole, and –CH<sub>2</sub>–imidazole–<sup>γ</sup>N–Bn. Attempts to isolate the metal insertion products with NiBr<sub>2</sub> and the closely related ligands **8**, **9**, **10**, and **11** failed (Figure 2).

The kinetics of Ni(II) insertion, although observable at RT by spectrophotometric methods (Figure 3), is complex. For NiBr<sub>2</sub> at 60 °C in MeOH using pseudo-first-order conditions,<sup>12</sup> the initial rate of insertion was ~10<sup>–4</sup> mol/min with a large excess **6f**, which slowed to ~10<sup>–6</sup> mol/min within 2–3 h of reaction. The rate of insertion is retarded by excess Ni<sup>2+</sup> ions and is enhanced by the addition of a weak base (NEt<sub>3</sub>, <sup>i</sup>Pr<sub>2</sub>NEt, DBU). Related work by Margerum and others with linear peptides indicates that the initially formed O,N amide Ni(II) complexes rearrange slowly to the more stable N,N amide complexes.<sup>13</sup> Interaction of the amide carbonyl with the imine-bound transition metals strongly acidifies the amide (δ–π back-bonding), but the factors which control

(12) Childers, R. F.; Wentworth, R. A. D. *Inorg. Chem.* **1969**, *8*, 2218–20.

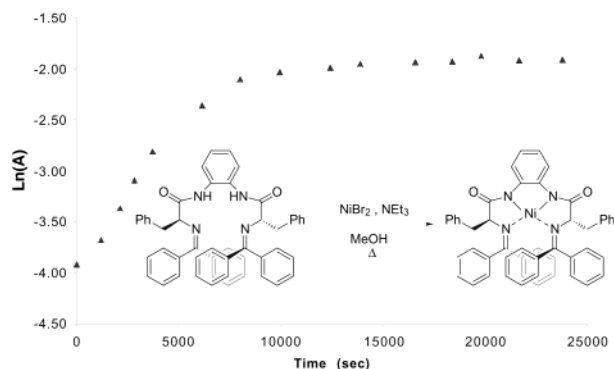


Figure 3. Ni(II) insertion at RT (370 nm).

Table 4. Isolated Metal Complexes

ligand	metal	color <sup>a</sup>	yield	complex
<b>6a</b>	NiBr <sub>2</sub>	maroon	71%	<b>7a·Ni<sup>II</sup></b>
<b>6k</b>	CoCl <sub>2</sub>	red <sup>c</sup>	79%	<b>7k·Co<sup>II</sup></b>
<b>6b</b>	NiBr <sub>2</sub>	maroon	86%	<b>7b·Ni<sup>II</sup></b>
<b>6f</b>	NiBr <sub>2</sub>	maroon	83%	<b>7f·Ni<sup>II</sup></b>
<b>6g</b>	NiBr <sub>2</sub>	text <sup>b</sup>	60%	<b>7g·Ni<sup>II</sup></b>
<b>6l</b>	NiBr <sub>2</sub>	maroon	96%	<b>7l·Ni<sup>II</sup></b>
<b>6k</b>	NiBr <sub>2</sub>	yellow	94%	<b>7k·Ni<sup>II</sup></b>
<b>6f</b>	CuCl <sub>2</sub>	violet	92%	<b>7f·Cu<sup>II</sup></b>
<b>6k</b>	CuCl <sub>2</sub>	green	95%	<b>7k·Cu<sup>II</sup></b>
<b>6f</b>	Et <sub>2</sub> Zn	none <sup>c</sup>	>90%	<b>7f·Zn</b>
<b>6f</b>	Me <sub>2</sub> Zn	none <sup>c</sup>	>90%	<b>7f·Zn</b>

<sup>a</sup> Solid state. <sup>b</sup> Crystals from CH<sub>2</sub>Cl<sub>2</sub> were maroon. Crystals from EtOAc/hexanes were dichroic. <sup>c</sup> Oil.

the subsequent O → N rearrangement are controlled by a number of effects that are complex and difficult to predict (e.g., steric demand of the ligand, additional ligation sites, oxophilicity of the metal). Because the O → N rearrangement must occur twice for each metal insertion, it is not likely that it will be possible to sort out kinetics for the discrete steps required for complete insertion of the metal.

Insertion of Ni(II), Cu(II), and Zn into **6f** to provide the corresponding complexes **7** was straightforward (Table 4). The Ni(II) and Cu(II) complexes were easily purified by column chromatography on SiO<sub>2</sub>. All of the complexes provided mass spectra with visible M<sup>+</sup> ions. The Ni(II) and Zn complexes were characterized by <sup>1</sup>H NMR, and several Ni(II) complexes were subjected to single-crystal X-ray analysis. The Cu(II) complexes provided good EPR spectra, with visible hyperfine couplings to the Cu, and superhyperfine couplings to the nitrogen ligands.

### Structure of the Complexes

The <sup>1</sup>H NMR spectra of the ligands (Table 5, Figure 6) showed downfield shifts upon insertion of Ni(II). In the cases where R<sup>1</sup> = R<sup>2</sup>, perfect C<sub>2</sub> symmetry was observed, as expected for a square planar complex. C<sub>2</sub> symmetry was *not* observed for the corresponding Zn complexes, and it is postulated that the Zn complexes are best described as square pyramidal.

A large downfield shift was observed for the equatorial α hydrogen of **7a·Ni<sup>II</sup>** (Figure 6, Table 5), which is probably due to the deshielding cone of an aromatic ring of N=CPh<sub>2</sub>, and not due to magnetic anisotropy introduced by the Ni(II) nucleus. A downfield shift is also observed for one of the β hydrogens of **7f·Ni<sup>II</sup>** and for *p*-MeO-**7f·Ni<sup>II</sup>**. This effect was not observed for the less hindered **7g·Ni<sup>II</sup>** and **7l·Ni<sup>II</sup>** side chains.

To gain some insight into the metal binding nature of the ligands, several Ni(II) complexes were subjected to single-crystal X-ray crystallography. In one case, a metal-free ligand (**11**) was subjected to crystallography for comparison (Figure 4). Interestingly, the three nitrogens appear to be somewhat pre-organized for metal binding. Because the Ph<sub>2</sub>C=N groups can hydrogen bond to the amide N–H, this causes all three nitrogens to become coplanar. It is noteworthy that the amino acid side chain is projected over the binding pocket for the metal.

Complex **7b·Ni<sup>II</sup>** provided maroon crystals from EtOAc/hexanes which were subjected to single-crystal X-ray analysis (Figure 5). It is noteworthy that the axial nature of the phenylalanine side chain observed in the ligand **11** is retained in this case, similar to what was observed for **7f·Ni<sup>II</sup>** and *p*-MeO-**7f·Ni<sup>II</sup>**, which have two phenylalanine side chains.<sup>7a</sup> With the exception of the phenylalanine side chain in **7b·Ni<sup>II</sup>**, this asymmetric complex still retains approximate C<sub>2</sub> symmetry with the distal Ph<sub>2</sub>C=N projecting above the plane on the same side as the side chain.

In all Ni(II) complexes studied by X-ray thus far, the complexes were approximately square planar, with average Ni–N bond lengths of 1.84 Å for the amide nitrogens, and 1.93 Å for the imine nitrogens (standard deviation <2%). The presence or absence of the *p*-methoxy group on the Schiff base moiety did not have a noticeable effect on bond lengths or other features in the ORTEP representations (Figures 7 and 8). Because several complexes crystallized with more than one unique molecule in the unit cell, there are more data here than the number of crystalline complexes would imply. The crystal packing of these complexes is interesting in its own right and will be reported elsewhere. All the Ni(II) complexes studied showed square planar geometry with an average tetrahedral distortion of 0.07 Å (0.011–0.137 Å, standard deviation = 0.040 Å, Table 6), as measured by how far N(4) is out of the plane defined by the first 3 nitrogens. This is a clear expression of the metal centered chirality. The overlapping Ar<sub>2</sub>C=N groups define a screw axis running through the metal, which has a predictable sense of helicity, or the ligand may even predetermine the sense of helicity.<sup>14</sup> That is, if the amino acids are S, then the metal-centered helicity is left-handed, or Λ. Indeed, this is apparent even in the less hindered tridentate ligand **11**, which does not even contain a metal.

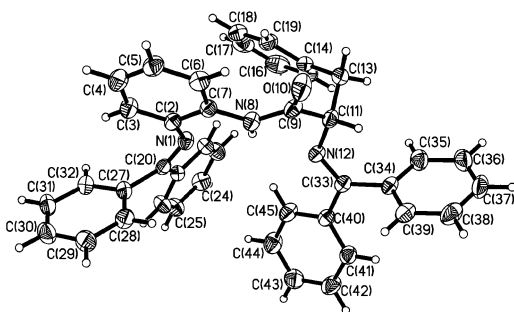
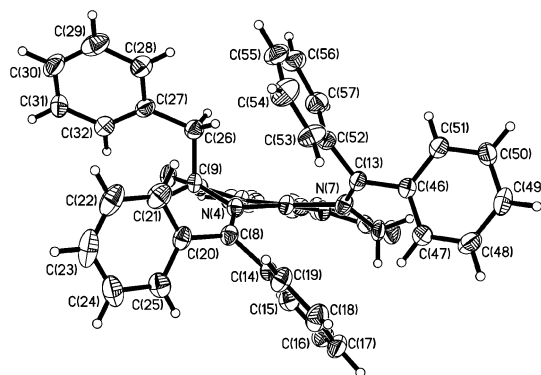
(13) (a) McDonald, M. R.; Fredericks, F. C.; Margerum, D. W. *Inorg. Chem.* **1997**, *36*, 3119–3124. (b) Kirvan, G. E.; Margerum, D. W. *Inorg. Chem.* **1985**, *24*, 3245–53. (c) Sigel, H.; Martin, R. B. *Chem. Rev.* **1982**, *82*, 385–426.

(14) (a) Mamula, O.; Von Zelewsky, A.; Bark, T.; Stoeckli-Evans, H.; Neels, A.; Bernardinelli, G. *Chem. Eur. J.* **2000**, *6*, 3575–85. (b) Muniz, K.; Bolm, C. *Chem. Eur. J.* **2000**, *6*, 2309–16. (c) Vázquez, M.; Bermejo, M. R.; Sanmartín, J.; García-Deibe, A. M.; Lodeiro, C.; Mahía, J. *J. Chem. Soc., Dalton Trans.* **2002**, 870–877.

**Table 5.** Effect of Ni(II) Insertion on Ligand Chemical Shifts and Coupling Constants

cmpd	residues	H( $\beta$ ) ( $\delta$ )	H( $\beta'$ ) ( $\delta$ )	H( $\alpha$ ) ( $\delta$ )	$J_{\beta\alpha}$ (Hz)	$J_{\beta'\alpha}$ (Hz)	$J_{\beta\beta'}$ (Hz)
<b>6a</b>	Gly, Gly			4.09			
<b>7a·Ni<sup>II</sup></b>	Gly, Gly			4.30 (ax) 3.56 (eq)			16.9 ( $J_{aa'}$ )
<b>6d</b>	Phe	3.14	3.35	4.29	9.7	3.0	12.9
	Ala	1.33		4.05	6.8		
<b>7d·Ni<sup>II</sup></b>	Phe	3.76	2.65	3.91	9.1	4.9	13.2
	Ala	1.69		3.62	6.8		
<b>6f</b>	Phe, Phe	3.12	3.29	4.23	9.2	3.3	13.1
<b>7f·Ni<sup>II</sup></b>	Phe, Phe	3.89	2.46	3.97	9.3	4.8	13.2
<b>6f<sub>p</sub>-MeO</b>	Phe, Phe	3.09	3.26	4.24	9.3	3.1	12.9
<b>7f<sub>p</sub>-MeO·Ni<sup>II</sup></b>	Phe, Phe	3.88	2.43	4.16	6.9	6.1	13.7
<b>6g<sup>a</sup></b>	Ser, Ser	~4.2–4.1	~3.8–3.7	~3.9	<i>a</i>	<i>a</i>	<i>a</i>
<b>7g·Ni<sup>II</sup></b>	Ser, Ser	4.08	3.72	3.60	4.7	4.5	11.2
<b>6l</b>	Ser(OAc)	4.44	4.29	4.26	6.8	6.4	13.1
	Ser(OAc)						
<b>7l·Ni<sup>II</sup></b>	Ser(OAc)	4.50	4.32	3.87	5.2	5.4	11.4
	Ser(OAc)						
<b>6j</b>	Phe	3.09	3.37	4.32	9.5	3.1	13.0
	His	2.66	2.93	4.11	5.2	5.1	14.8
<b>6k</b>	Phe	3.08	3.23	4.20	9.3	3.3	13.0
	BnHis	3.15	3.13	4.27	7.3	4.7	14.5

<sup>a</sup> Oxazolidine- $\beta$ -hydroxyimine tautomerism causes severe overlap in the case of **6g**. *J* values not determined.

**Figure 4.** ORTEP representation of ligand **11**.**Figure 5.** ORTEP representation of **7b·Ni<sup>II</sup>**, front view.

This same type of interaction has been observed in Cu(II) complexes by Borovik.<sup>15</sup>

The source of this chirality may be attributed to the extreme A<sup>1,3</sup> strain about the Ar<sub>2</sub>C=N-CH moiety, which has been observed in the context of the observed weak acidity of the  $\alpha$  proton.<sup>16</sup>

Unfortunately, none of the Cu(II) complexes crystallized in a form that was suitable for X-ray analysis. Because the d<sup>9</sup> Cu(II) complexes complicate NMR analysis, an electron spin resonance (ESR) study of **7f·Cu<sup>II</sup>** and **7k·Cu<sup>II</sup>** (Figure 9) was performed. Because the colors of these two complexes were quite different (violet for the tetracoordinate **7f·Cu<sup>II</sup>**, and green for **7k·Cu<sup>II</sup>**), it was obvious from the start that

the ligand environment was different for these two complexes. Continuous wave (CW, X-band) ESR spectra were recorded of both Cu(II) complexes in a frozen solution of CH<sub>2</sub>Cl<sub>2</sub> at 77 K (Figure 10). Both showed the hyperfine coupling and *g*-values expected for Cu(II) in similar pseudoplanar N<sub>4</sub> complexes<sup>17</sup> ( $g_{\perp} = 2.01, 1.97$ ,  $g_{\parallel} = 2.22, 2.19$ ;  $A_{zz} \sim 400$  and 500 MHz for **7k·Cu<sup>II</sup>** and **7f·Cu<sup>II</sup>**, respectively), but whereas the superhyperfine coupling to the nitrogen ligands was quite distinct for **7f·Cu<sup>II</sup>**, the superhyperfine coupling was obscure for the pentacoordinate case **7k·Cu<sup>II</sup>**.

Obviously, the loss of resolution reflects the fact that hyperfine/quadrupole parameters of the four strongly coupled <sup>14</sup>N are less equivalent in **7k·Cu<sup>II</sup>** than those of **7f·Cu<sup>II</sup>**. To qualitatively understand this difference, we performed pulsed ENDOR measurements of <sup>14</sup>N for both complexes. The sets of ENDOR spectra acquired in various positions of the EPR spectra are shown in the Supporting Information.

The ENDOR spectra of **7f·Cu<sup>II</sup>** and **7k·Cu<sup>II</sup>** were acquired at a single selective low field position ( $g_{\parallel}, m_1 = -3/2$ ) (Figure 11). In both cases, ENDOR spectra are spread between 10 and 25 MHz and show 5–4 distinctive peaks. In this particular field position, we can neglect the disorder due to molecular orientation and evaluate the hyperfine/quadrupole parameters (Table 7).<sup>18</sup>

- (15) Kawamoto, T.; Hammes, B. S.; Haggerty, B.; Yap, G. P. A.; Rheingold, A. L.; Borovik, A. S. *J. Am. Chem. Soc.* **1996**, *118*, 285–6.
- (16) O'Donnell, M. J.; Bennett, W. D.; Bruder, W. A.; Jacobsen, W. N.; Knuth, K.; LeClef, B.; Polt, R. L.; Bordwell, F. G.; Mrozack, S. R.; Cripe, T. A. *J. Am. Chem. Soc.* **1988**, *110*, 8520–5.
- (17) (a) *Advanced EPR, Applications in Biology and Biochemistry*; Hoff, A. J., Ed.; Elsevier: Amsterdam, 1989. (b) See examples in: Pilbrow, J. R. *Transition Ion Electron Paramagnetic Resonance*; Clarendon Press: Oxford, 1990; Chapters 5 and 11. (c) Brown, T. G.; Hoffman, B. M. *Mol. Phys.* **1980**, *39*, 1073. (d) Goldfarb, D.; Fauth, J.-M.; Tor, Y.; Shanzer, A. *J. Am. Chem. Soc.* **1991**, *113*, 1941–8. (e) Van Dam, P. J.; Reijerse, E. J.; Van Der Meer, M. J.; Guajardo, R.; Mascharak, P. K.; De Boer, E. *Appl. Magn. Reson.* **1996**, *10*, 71–86. (f) Bender, C. J.; Peisach, J. *J. Chem. Soc., Faraday Trans.* **1998**, *94*, 375–386. (g) Slutter, C. E.; Gromov, I.; Epel, B.; Pecht, I.; Richards, J. H.; Goldfarb, D. *J. Am. Chem. Soc.* **2001**, *123*, 5325–5336.
- (18) Details may be found in the Supporting Information.

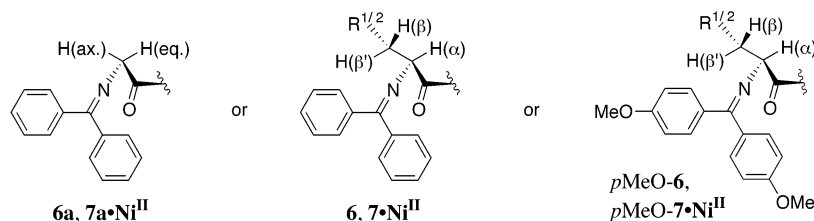


Figure 6. ABX spectra provided by H( $\alpha$ ), H( $\beta$ ), and H( $\beta'$ ) for ligands and complexes.

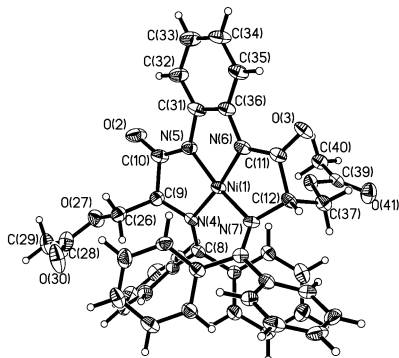


Figure 7. ORTEP representation of **7l**•Ni<sup>II</sup>, top view.

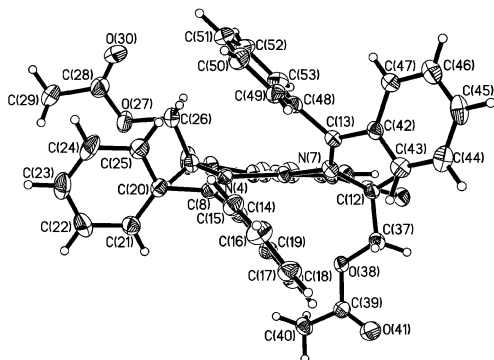


Figure 8. ORTEP representation of **7l**•Ni<sup>II</sup>, side view.

In both complexes, there are two groups of two <sup>14</sup>N with approximate parameters,  $A \sim 28\text{--}30$  MHz and  $A \sim 39\text{--}41$  MHz, which shows that structures of **7f**•Cu<sup>II</sup> and **7k**•Cu<sup>II</sup> are, in general, similar. In accordance with Iwaizumi et al.,<sup>19</sup> the hyperfine interaction of 38–48 MHz correspond to  $sp^2$  nitrogens, while those of 33–27 MHz correspond to  $sp^3$  nitrogens ligated to Cu(II). Both types of nitrogens are easily seen in complex structure.

In principle, more structural information can be obtained from the evaluated parameters of quadrupole interaction because the axes of the quadrupole tensor and the direction of the metal–N bonds are interrelated.<sup>20</sup>

The magnitude of the principal elements of the quadrupole tensor  $Q_0$  and the asymmetry parameter  $\eta$  of the metal bound ligand and corresponding free ligand can, however, be substantially different. For instance, the numerous studies of planar metal porphyrin complexes<sup>21</sup> have shown that the main axis of the quadrupole tensor can be either parallel or perpendicular to the Cu–N bond, albeit remaining in a porphyrin plane. In addition, in this work, the parameters of

the quadrupole interactions were determined in the  $g$ -frame, and the relation between the  $g$ -frame and the molecular frame requires work that is beyond the scope of this paper. On the basis of the observed values of the quadrupole interactions, we can only make some qualitative conclusions about the structure of **7f**•Cu<sup>II</sup> and **7k**•Cu<sup>II</sup>. Assuming that all nitrogens have a similar quadrupole tensor, that the  $z$ -axis of the quadrupole tensor is directed along the Cu–N bond, and that the asymmetry parameter  $\eta$  is  $\sim 0.5$ , one can estimate that the angle between the  $xy$ -plane of the  $g$ -frame and the Cu–N bond of the imine nitrogens in **7k**•Cu<sup>II</sup> is  $30\text{--}50^\circ$ . If we then assume that the value of the  $Q_0$  element of the quadrupole tensor is about 4 MHz,<sup>22</sup> we can determine that the amide nitrogens are closer to the  $xy$ -plane of  $g$ -frame, making this angle  $0\text{--}20^\circ$ . All these data show that both complexes are not planar.

Because of the low magnetic momentum of <sup>14</sup>N, pulsed ENDOR is not appropriate for the investigation of weakly coupled <sup>14</sup>N ligands. Therefore, to examine the presence of the fifth (axial or apical?) coordinated nitrogen in **7k**•Cu<sup>II</sup>, we applied electron spin–echo envelope modulation, which is suitable for the investigation of the weakly coupled Cu–<sup>14</sup>N. As shown, the ESEEM measurements were performed in various positions of the EPR spectrum. For the sake of comparison, similar measurements were performed for **7f**•Cu<sup>II</sup>, where the fifth coordinated <sup>14</sup>N was not present. The ESEEM measurements of **7k**•Cu<sup>II</sup> clearly showed the modulation related to <sup>14</sup>N, and those of **7f**•Cu<sup>II</sup> did not. The FT ESEEM spectra for the mostly nonselective field position for these two compounds are shown in Figure 12.

While the spectrum of **7f**•Cu<sup>II</sup> does not show any <sup>14</sup>N related lines, the FT spectrum of **7k**•Cu<sup>II</sup> shows 4 lines, typical for weakly coupled <sup>14</sup>Ns under so-called “cancellation conditions”. From line positions, one can immediately evaluate a hyperfine interaction constant of 1.5–2.0 MHz and parameters of quadrupole interactions: nuclear quadrupole coupling constant of 0.75 MHz and an asymmetry parameter of 0.3–0.4. These values are quite typical for <sup>14</sup>N. Therefore, ESEEM data unambiguously show that **7k**•Cu<sup>II</sup> is a pentacoordinate complex.

### Redox Behavior of **7f**•Cu<sup>II</sup> and **7f**•Ni<sup>II</sup>

Atom transfer reactions seemed to be an obvious application of the Schiff base ligand system. Thus, we wished to examine the ability of this ligand to support higher oxidation

(19) Iwaizumi, M.; Kudo, T.; Kita, S. *Inorg. Chem.* **1986**, 25, 1546–50.

(20) Jiang, F.; Karlin, K. D.; Peisach, J. *Inorg. Chem.* **1993**, 32, 2576–82.

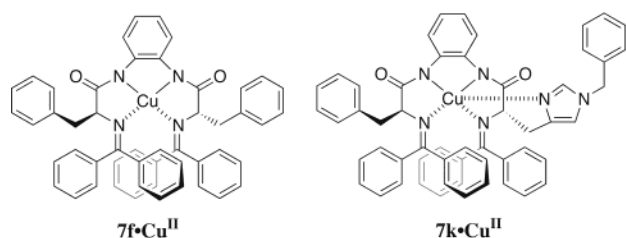
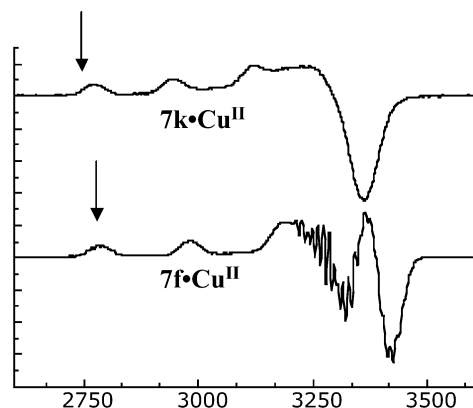
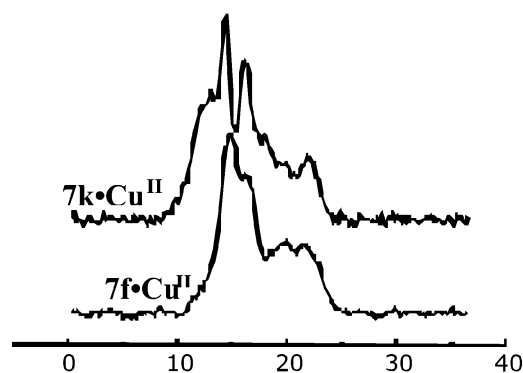
(21) Van Doorslaer, S.; Bachmann, R.; Schweiger, A. *J. Phys. Chem. A* **1999**, 103, 5446–5455 and references therein.

(22) *Electron Spin–Echo Envelope (ESEEM) Spectroscopy*; Dikanov, S. A., Tsvetkov, Yu. D., Eds.; CRC Press: Boca Raton, FL, 1992.

**Table 6.** Summary of Ni(II) Ligation from X-ray Data

complex	R <sup>1</sup>	R <sup>2</sup>	R <sup>3</sup>	N <sup>1</sup> –Ni (Å)	N <sup>2</sup> –Ni (Å)	N <sup>3</sup> –Ni (Å)	N <sup>4</sup> –Ni (Å)	distortion <sup>a</sup> (Å)
<b>7b</b> •Ni <sup>II</sup>	H	CH <sub>2</sub> Ph	H	1.922(2)	1.906(2)	1.833(2)	1.833(2)	0.100
<i>p</i> -MeO- <b>7b</b> •Ni <sup>II</sup>	H	CH <sub>2</sub> Ph	OCH <sub>3</sub>	1.915(7)	1.909(7)	1.829(7)	1.821(7)	0.128
<i>b</i> <sup>7f</sup> •Ni <sup>II</sup>	CH <sub>2</sub> Ph	CH <sub>2</sub> Ph	H	1.944(4)	1.942(4)	1.843(5)	1.830(4)	0.026
<i>c</i> <sup>7f</sup> •Ni <sup>II</sup>	CH <sub>2</sub> Ph	CH <sub>2</sub> Ph	H	1.921(5)	1.963(5)	1.843(5)	1.849(5)	0.137
<i>p</i> -MeO- <b>7f</b> •Ni <sup>II</sup>	CH <sub>2</sub> Ph	CH <sub>2</sub> Ph	OCH <sub>3</sub>	1.9479 (17)	1.9329 (18)	1.8455 (18)	1.8442 (17)	0.066
<i>rac</i> - <b>7g</b> •Ni <sup>II</sup>	CH <sub>2</sub> OH	CH <sub>2</sub> OH	H	1.943(3)	1.922(3)	1.834(3)	1.840(3)	0.011
<b>CH<sub>2</sub>Cl<sub>2</sub> 7g</b> •Ni <sup>II</sup>	CH <sub>2</sub> OH	CH <sub>2</sub> OH	H	1.957(2)	1.903(3)	1.837(3)	1.846(2)	0.066
<b>7l</b> •Ni <sup>II</sup>	CH <sub>2</sub> OAc	CH <sub>2</sub> OAc	H	1.963(3)	1.925(3)	1.829(3)	1.852(3)	0.071
<i>c</i> <sup>7l</sup> •Ni <sup>II</sup>	CH <sub>2</sub> OAc	CH <sub>2</sub> OAc	H	1.968(3)	1.921(3)	1.845(3)	1.846(3)	0.068

<sup>a</sup> Out-of-plane distortion of one N<sup>4</sup> relative to N<sup>1</sup>–N<sup>3</sup>. <sup>b</sup> C<sub>2</sub>-symmetric complex. <sup>c</sup> Non-C<sub>2</sub>-symmetric complex. Complexes **7f**•Ni<sup>II</sup> and **7l**•Ni<sup>II</sup> crystallize with two molecules per unit cell, which differ principally by a rotation about  $\chi_1$  of one of the side chains.<sup>7a</sup>

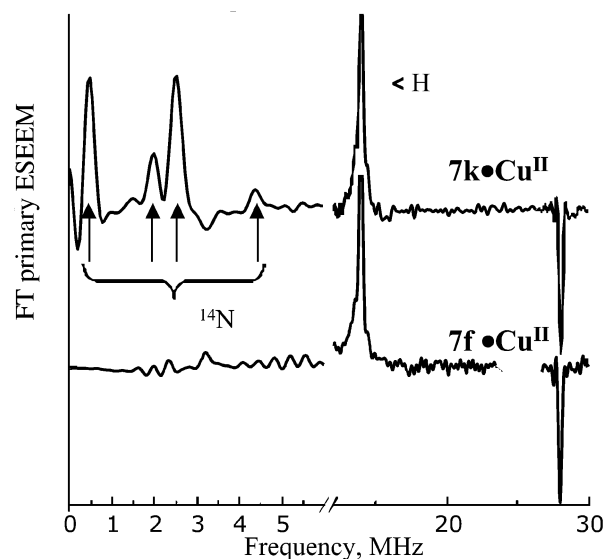
**Figure 9.** Cu(II) complexes for ESR study.**Figure 10.** First derivative CW spectrum of **7f**•Cu<sup>II</sup>. First derivative X-band EPR spectra of **7k**•Cu<sup>II</sup> and **7f**•Cu<sup>II</sup>. Arrows show field positions (Gauss) where pulsed ENDOR measurements were obtained (Figure 11). Dashed lines show field positions for ESEEM measurements (Figure 12).**Figure 11.** Pulsed ENDOR spectra of Cu(II) complexes. Davies ENDOR spectra of **7k**•Cu<sup>II</sup> and **7f**•Cu<sup>II</sup> acquired in most selective field positions, shown in Figure 10 by arrows. Microwave frequency = 9.421 MHz; microwave pulse durations = 30 ns, 15 ns, 30 ns; RF pulse duration = 5  $\mu$ s; nominal RF power  $\sim$  1 kW;  $\tau$  = 450 ns;  $T$  = 13 K; pulse repetition rate = 200 Hz.

states of transition metals. The reversible nature of the II/III redox of copper and nickel suggested that these complexes may be of value in catalysis.

**Table 7.** Hyperfine and Quadrupole Parameters<sup>a</sup>

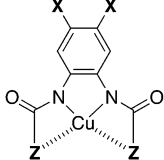
<b>7f</b> •Cu <sup>II</sup>			
A <sub>1</sub>	A <sub>2</sub>	A <sub>3</sub>	A <sub>4</sub>
41 MHz	39.2 MHz	31.2 MHz	30.6 MHz
P <sub>1</sub>	P <sub>2</sub>	P <sub>3</sub>	P <sub>4</sub>
1.06 MHz	1.06 MHz	0 MHz	0 MHz
<b>7k</b> •Cu <sup>II</sup>			
A <sub>1</sub>	A <sub>2</sub>	A <sub>3</sub>	A <sub>4</sub>
40.5 MHz	38.5 MHz	29 MHz	28 MHz
P <sub>1</sub>	P <sub>2</sub>	P <sub>3</sub>	P <sub>4</sub>
1.2 MHz	1.2 MHz	0.5 MHz	0.82 MHz

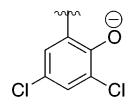
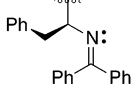
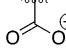
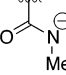
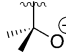
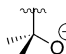
<sup>a</sup> Hyperfine and quadrupole parameters of <sup>14</sup>N (<sup>14</sup>N A<sub>zz</sub> and <sup>14</sup>N P<sub>zz</sub>) evaluated from ENDOR spectra at  $g_{||}$ ,  $m_I = -3/2$ . The details are shown in Supporting Information.

**Figure 12.** ESEEM spectra for **7k**•Cu<sup>II</sup> and **7f**•Cu<sup>II</sup>. Cosine FT primary ESEEM of **7f**•Cu<sup>II</sup> and **7k**•Cu<sup>II</sup> acquired in the most nonselective field positions (Figure 10). Experimental conditions: mw frequency = 9.421; mw pulse durations = 2  $\times$  10 ns;  $\tau_0$  = 200 ns;  $T$  = 13 K.

Amide ligands are known to stabilize higher oxidation states (e.g., Ni(III) and Cu(III)).<sup>23</sup> Cyclic voltammetry of **7f**•Cu<sup>II</sup> showed a highly reversible II/III couple similar to what was observed by Ruiz<sup>24</sup> and others<sup>25</sup> with tetracoordinate copper complexes derived from substituted *o*-phenylenediamines (Table 8). The corresponding Ni(II)/(III) couple for **7f**•Ni<sup>II</sup> was also reversible, with  $E/V = +0.52$  V. Although

- (23) Bour, J. J.; Birker, J. P. M. W. L.; Steggerda, J. J. *Inorg. Chem.* **1971**, *10*, 1202–5.  
 (24) Ruiz, R.; Surville-Barland, C.; Aukauloo, A.; Anxolabehere-Mallart, E.; Journaux, Y.; Cano, J.; Munoz, M. C. *J. Chem. Soc., Dalton Trans.* **1997**, 745–751.

**Table 8.** *E/V* Values for Cu(II)/(III) in CH<sub>3</sub>CN


X	Z	<i>E/V</i>
Cl—		+ 0.51 <sup>a</sup>
H—		+ 0.44 <sup>b</sup>
H—		+ 0.41 <sup>c</sup>
H—		- 0.02 <sup>c</sup>
Cl—		- 0.44 <sup>a</sup>
H—		- 0.47 <sup>a</sup>

<sup>a</sup> Reference 23. <sup>b</sup> This work. <sup>c</sup> Reference 22.

Ni(IV)=O species have been suggested as putative intermediates in nickel catalyzed oxygen atom transfer reactions,<sup>26</sup> results from epoxidation studies support Ni(III)—O• as a more likely intermediate, especially in light of the observed

- (25) Anson, F. C.; Collins, T. J.; Richmond, T. G.; Santarsiero, B. D.; Toth, J. E.; Treco, B. G. R. T. *J. Am. Chem. Soc.* **1977**, *99*, 4527.  
 (26) (a) Yoon, H.; Wagler, T. R.; O'Connor, K. J.; Burrows, C. J. *J. Am. Chem. Soc.* **1990**, *112*, 4568–70. (b) Fernandez, I.; Pedro, J. R.; Rosello, A. L.; Ruiz, R.; Ottenwaelde, X.; Journaux, Y. *Tetrahedron Lett.* **1998**, *39*, 2869–2872.

irreversibility of the Ni III/IV oxidation states. The *trans*-epoxides were the major product in every case, regardless of the starting olefin geometry.<sup>27</sup>

## Conclusions

The stability of the complexes and the variety of metals accepted by the Schiff base ligands, coupled with the simplicity of their synthesis and the widespread availability of enantiomerically pure amino acids of either R or S configuration, suggests that these ligands may be considered “privileged”. Future work in this laboratory will revolve around the use of these ligands in solution and in their resin-bound forms to develop new enantioselective catalysts for oxidations and carbon–carbon bond formation.

**Acknowledgment.** We thank the National Science Foundation (Grants CHE-9201112, CHE-9526909 and CHE-9729350) for partial support of this work and for the provision of the X-ray diffraction apparatus (Grant CHE-9610374). R.E.R. is a DuPont-Arizona Research Experience undergraduate fellowship recipient.

**Supporting Information Available:** X-ray crystallographic files in CIF format (for **7b**•Ni<sup>II</sup>, *p*-MeO-**7b**•Ni<sup>II</sup>, **7f**•Ni<sup>II</sup>, *p*-MeO-**7f**•Ni<sup>II</sup>, *rac*-**7g**•Ni<sup>II</sup>, CH<sub>2</sub>Cl<sub>2</sub>-**7g**•Ni<sup>II</sup>, **7i**•Ni<sup>II</sup>, **11**). ESR details for **7f**•Cu<sup>II</sup>, **7k**•Cu<sup>II</sup>, **7k**•Co<sup>II</sup>, and **7k**•Mn<sup>II</sup>. This material is available free of charge via the Internet at <http://pubs.acs.org>.

IC0259960

- (27) The oxidation of simple *cis*- and *trans*-olefins was examined using complex **7f**•i<sup>II</sup> and NaOCl (commercial bleach) as an oxidant. [Meunier, B.; Guilmet, E.; De Carvahlo, M. E.; Poilblanc, R. *J. Am. Chem. Soc.* **1984**, *106*, 6668–9.] No attempt was made to optimize these reactions. While the ee's were not large (~4%), turnover numbers of 12–14 with *trans*-β-methylstyrene and **7f**•Ni<sup>II</sup> indicate that the ligand system can function under the strongly oxidizing conditions of catalysis. In several cases, the unchanged catalyst could be recovered after the reaction. Other oxidants were also surveyed. PhI=O was also effective as an oxidant, but NaIO<sub>4</sub> and H<sub>2</sub>O<sub>2</sub> were not. [Kinneary, J. F.; Wagler, T. R.; Burrows, C. J. *Tetrahedron Lett.* **1988**, *29*, 877–80.]